Multidisciplinary Materials Chronicles, 2025, Vol. X, Iss. X, 140-149

DOI: 10.62184/mmc.jmmc1100202532

Research Article

SCIENCE PARK PUBLISHER

Multidisciplinary Materials Chronicles

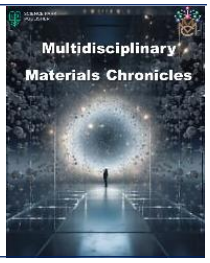

Plasma dynamics and surface interaction in a DC Ar-N_2 hollow cathode discharge system: Insights from optical emission spectroscopy

A.E. Metawa[1,2], Marwa Karim[3], A.M. Hassan[4,*]

[1] Physics Department, Faculty of Science, Al-Baha University, Saudi Arabia

[2] Physics Department, Faculty of Science, Al-Azhar University, Cairo, Egypt

[3] Physics Department, Faculty of Science, Alexandria University, Moharram Bek, P.O. Box 21511, Alexandria, Egypt

[4] Physics Department, Faculty of Science, Al-Azhar University, Assiut, Egypt

Received: 30, 07, 2025; Accepted: 26, 11, 2025; Published: 14, 12, 2025

Abstract

This study investigates the optical properties of an Ar/N_2 plasma system, aiming to understand excitation and vibrational dynamics under various discharge conditions. Using optical emission spectroscopy, the effects of gas composition and discharge voltage on spectral features were systematically examined. The introduction of Ar into the mixture was found to significantly enhance the intensity of atomic emission lines, indicating its role in promoting electron excitation processes. In contrast, the vibrational bands of N_2 were strongly dependent on the fraction of nitrogen in the mixture, reflecting its dominant contribution to vibrational energy transfer. The interplay between Ar and N_2 highlights important mechanisms of collisional excitation and de-excitation in mixed-gas plasmas. The results suggest that controlling the Ar/N_2 ratio provides an effective means to tailor plasma characteristics, where Ar improves excitation efficiency while N_2 governs vibrational dynamics. Such insights are particularly relevant for applications in plasma-assisted surface modification and thin film deposition, where precise control of plasma parameters is required. This work, therefore, contributes to a better understanding of energy transfer pathways in mixed-gas plasmas and establishes a foundation for further investigations using advanced optical diagnostics.

Keywords: Hollow cathode discharge; Optical emission spectroscopy; Second positive system; First negative system

1. Introduction

Hollow cathode discharges represent a distinct form of plasma generation in which a plasma jet is produced within a hollow tube and propagates from the cathode toward the anode. This type of discharge has found widespread application in numerous plasma-based devices, including electron sources, ion thrusters, and materials processing systems [1–3]. One notable application of the hollow cathode effect lies in its utility for thin film deposition, where it offers enhanced ionization efficiency and localized plasma generation [4]. In particular, the nozzle-based hollow cathode plasma jet system serves as a highly effective source of directed plasma streams, which, under certain operating conditions, can reach supersonic velocities [5, 6].

The underlying mechanism of the hollow cathode effect involves two interrelated physical processes. Initially, electrons accelerated by the applied discharge voltage undergo multiple oscillations between the opposing inner surfaces of the hollow cathode [7]. These "pendulum electrons" acquire significant energy and contribute to the excitation and ionization of the working gas through inelastic collisions [8]. Concurrently, relaxation processes within the cathode

Multidisciplinary Materials Chronicles, 2025, Vol. X, Iss. X, 140-149

DOI: 10.62184/mmc.jmmc1100202532

Research Article

geometry give rise to photon emission, while energetic ions and metastable species bombard the cathode walls, enhancing secondary electron emission and sustaining the discharge.

Moreover, the interaction of energetic gas ions, such as those of oxygen or nitrogen, with the inner surfaces of the nozzle leads to the formation of compound films (e.g., oxides and nitrides) through surface reactions [9]. These films, along with material sputtered from the cathode or nozzle walls, become entrained in the plasma jet and subsequently transported toward the substrate, facilitating the formation of thin films. Importantly, both elemental materials and chemically complex cathodes, including ceramics and compounds, can be utilized depending on the desired film composition [10].

For diagnostic and analytical purposes, optical emission spectroscopy (OES) has emerged as a powerful and non-invasive technique to characterize the properties of plasma systems [11]. OES enables the identification of atomic and molecular species, as well as the evaluation of energetic parameters such as electron temperature [T_{exc} and T_{vib}] and excitation states [12]. One commonly employed method to determine these parameters is the Boltzmann plot technique, which relies on the analysis of emission intensities from excited states [13]. Electrons within the plasma, energized by the applied electromagnetic field, undergo collisions with gas particles. Inelastic collisions promote atoms or molecules to excited states, from which they decay and emit characteristic photons [14]. The emitted light intensity is directly related to the population of the upper energy levels and, by extension, reflects the energy distribution of electrons in the plasma [15]. In this work, an Ar-N_2 gas mixture plasma is characterized using optical emission spectroscopy to analyze its excitation and vibrational properties. Special attention is given to the effect of argon admixture on the vibrational temperature of the nitrogen second positive system, providing insight into energy transfer mechanisms and population dynamics in mixed-gas discharges.

2. Theoretical background

2.1. Emission intensity and population density

The relationship between the intensity of emitted radiation at a specific wavelength and the population density of particles in the excited state is given by the following expression as in equation (1) [16, 17]:

$$I_{\upsilon'\upsilon''} = C(\lambda_{\upsilon'\upsilon''})h\upsilon_{\upsilon'\upsilon''}A_{\upsilon'\upsilon''}n_{\upsilon'} \quad (1)$$

Where $C(\lambda_{\upsilon'\upsilon''})$ is a proportionality constant that includes the spectral sensitivity of the detection system and the geometrical factors of the optical setup, h is the Planck's constant, $\upsilon_{\upsilon'\upsilon''}$ is the frequency corresponding to the transition, $A_{\upsilon'\upsilon''}$ is the Einstein coefficient for spontaneous emission and $n_{\upsilon'}$ is the population density of the upper energy level (e.g., the $C^3\Pi_u(\upsilon')$ vibrational state in N_2). where, C_3 indicates the molecular symmetry classification, part of the C_3v point group, Π represents the orbital angular momentum of the electrons, indicating the orientation of the electron cloud, u denotes that the state is ungraded, meaning it is not symmetric with respect to inversion through the center of the molecule, and (υ') indicates the vibrational level associated with this electronic state, where υ' can take various integer values representing different vibrational energy levels.

2.2. The excitation temperature of the Ar plasma

The electron excitation temperature (T_{exc}) is a key parameter that reflects the energy distribution of electrons populating excited atomic or molecular states [18, 19]. It is important to note that T_{exc} is not necessarily equivalent to the electron temperature (T_e), particularly in non-equilibrium plasmas. The excitation temperature can be estimated using the Boltzmann plot method, according to the following relation, as in equation (2) [19]:

$$\ln\left(\frac{I_{ki}\lambda_{ki}}{g_k A_{ki}}\right) = -\frac{E_k}{KT_{exc}} + C \quad (2)$$

Where I_{ki}, λ_{ki}, g_k, A_{ki}, E_k ,and K are the measured line intensity, the emission wavelength, the statistical weight of the upper energy level, the transition probability (Einstein coefficient), the energy of the upper level, and Boltzmann's constant, respectively [20].

2.3. Spectrum of the N_2 second positive system (SPS)

The SPS of molecular nitrogen corresponds to the electronic transition from the excited state $C^3\Pi_u$ to $B^3\Pi_g$. The ground-state N_2 molecule, N_2 ($X^1\sum^+_g$) can be excited to the $C^3\Pi_u$ state via various mechanisms [21], including:

1- Electron impact excitation is illustrated in equation (3):

$$N_2(X^1\sum\nolimits_g^+) + e^- \rightarrow N_2(C^3\prod\nolimits_u) \quad (3)$$

Multidisciplinary Materials Chronicles, 2025, Vol. X, Iss. X, 140-149

DOI: 10.62184/mmc.jmmc1100202532

Research Article

2- Recombination of a nitrogen ion and an electron is illustrated in equation (4):

$$N_2^+ + e^- \rightarrow N_2(C^3\prod_u) \qquad (4)$$

The population of the vibrational levels in the $C^3\Pi_u$ state can be determined from the measured intensities of the vibrational bands in the SPS. Several assumptions are typically made in determining the vibrational temperature (T_{vib}) [22]:

- The $C^3\Pi_u(\upsilon') \rightarrow B^3\Pi_g$ (υ'') transition is predominantly excited via electron impact, Penning ionization, and pooling reactions.
- The vibrational level populations in the C state follow the Franck-Condon principle.
- For small changes in vibrational quantum numbers, the populations approximately follow the Boltzmann distribution.

Additional pathways that contribute to the excitation of the $C^3\Pi_u$ state include equations (5) and (6) [23, 24]:

$$N_2(X^1\sum_g^+) + e^- \rightarrow N_2(A^3\sum_u^+) \qquad (5)$$

$$N_2(A^3\sum_u^+) + e^- \rightarrow N_2(C^3\prod_u) \qquad (6)$$

The SPS band dominates the 300-490 nm spectral range and is commonly observed in nitrogen-containing discharges [25]. The emission intensity of these bands generally increases with the population density of the excited state, especially when driven by electron impact or two-step excitation mechanisms [26].

2.4. Vibrational temperature determination

The vibrational temperature (T_{vib}) of molecular nitrogen in the $C^3\Pi_u$ state can be evaluated using the Boltzmann plot method based on the measured intensities of individual vibrational bands. The relationship is expressed as in equation (7) [27]:

$$\ln\left(\frac{I_{\upsilon'\upsilon''}}{q\upsilon^4}\right) = C - \frac{E_{\upsilon'}}{kT_{vib}} \qquad (7)$$

Where $I_{\upsilon'\upsilon''}$ is the emission intensity of the band corresponding to the $\upsilon' \rightarrow \upsilon''$ vibrational transition, q is the Franck-Condon factor, υ is the frequency of the band head, $E_{\upsilon'}$ is the vibrational energy of the upper state, k is Boltzmann's constant, and C is a constant.

3. Experimental setup

A schematic diagram of the DC hollow cathode discharge system is shown in Figure 1. The system comprises a DC power supply (0-2 kV), a discharge cell, and an optical diagnostic setup. The plasma is generated inside a cylindrical hollow cathode with an inner radius of 0.3 cm, and the discharge extends toward a circular anode with a diameter of 1.25 cm. The discharge chamber itself is a stainless-steel cylinder, 20 cm in length and 2 cm in inner radius. The electrode separation, i.e., the gap between the hollow cathode and the anode plate, is fixed at 2 cm. Vacuum is achieved using an Edwards rotary pump coupled with a silicone oil diffusion pump, allowing a base pressure down to 5×10^{-6} Torr. The working gas mixture, consisting of a mixture of argon and nitrogen (Ar/N_2 = 50: 50%), is introduced into the chamber through independently regulated mass flow controllers (Tylan General), allowing precise adjustment of the mixing ratios. The gas pressures were varied to 25, 50, 75, and 100 mTorr, monitored and regulated using a Pirani Penning gauge (model 1005).

Optical emission spectroscopy (OES) was employed to diagnose the discharge. Spectral emissions from Ar and N_2 species were recorded using a monochromator (model 77200) operating over the 300-900 nm wavelength range. The monochromator has a focal length of 35 cm, equipped with a diffraction grating of 1200 grooves/mm, offering a spectral resolution better than 0.2 Å. The output signal was detected using a photomultiplier tube (PMT, model 9558QB) for enhanced sensitivity.

4. Results and discussion

4.1. Ar excitation temperature

Figure 2 shows the identification of Ar emission lines recorded in the wavelength range of 400-445 nm from a mixture of Ar/N_2 plasma generated via DC hollow cathode discharge operated at a gas pressure of 100 mTorr and an applied voltage of 1.5 kV (as an example). The excitation temperature (T_{exc}) was determined from these spectral lines using the Boltzmann plot method (Equation 2).

Figures 3a and 3b display the Boltzmann plots of $ln(I\lambda/gA)$ versus the upper energy level E for Ar lines at applied voltage 1.5 kV and gas pressures of 100 mTorr and at applied voltage

Multidisciplinary Materials Chronicles, 2025, Vol. X, Iss. X, 140-149
DOI: 10.62184/mmc.jmmc1100202532

Research Article

0.5 kV and 25 mTorr, respectively.

Figures 4a and 4b illustrate the determination of excitation temperatures from the inverse slopes of the fitted lines. As shown in Figure 4a, T_{exc} decreases from 0.381 eV to 0.226 eV as the gas pressure increases from 25 mTorr to 100 mTorr. This decrease is attributed to an increase in ground-state neutral atom density (n_0) and electron density (n_e), both of which contribute to higher collisional de-excitation rates, thereby reducing the effective excitation temperature [28].

On the other hand, Figure 4b demonstrates the influence of applied voltage on T_{exc}. As the applied voltage increases from 0.5 kV to 1.5 kV, the excitation temperature increases from 0.226 eV to 0.381 eV, due to the higher energy gain by electrons from the electric field, leading to more effective excitation processes [29].

4.2. Intensity of the SPS and FNS of N_2 spectra

Figures 5a and 5b show the optical emission spectra identifying the Second Positive System (SPS) and First Negative System (FNS) of nitrogen gas. Figure 5a presents the spectrum obtained at 25 mTorr and 1.0 kV (as an example).

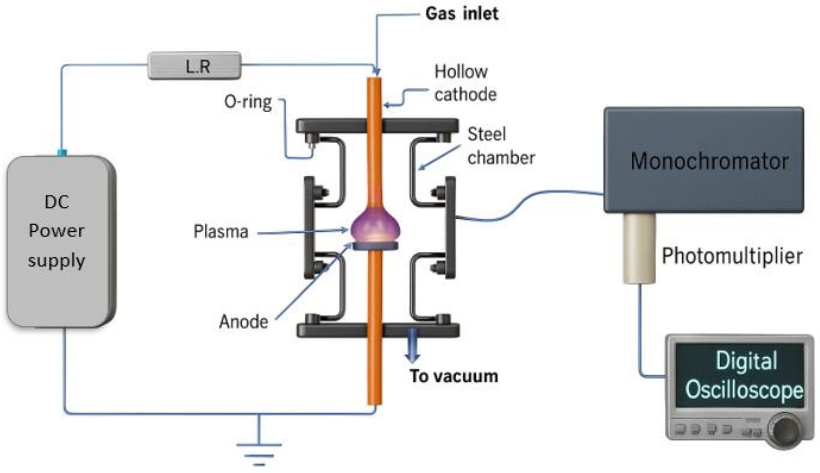

Figure 1. Schematic diagram of the DC hollow cathode system and optical emission spectroscopy (OES) system.

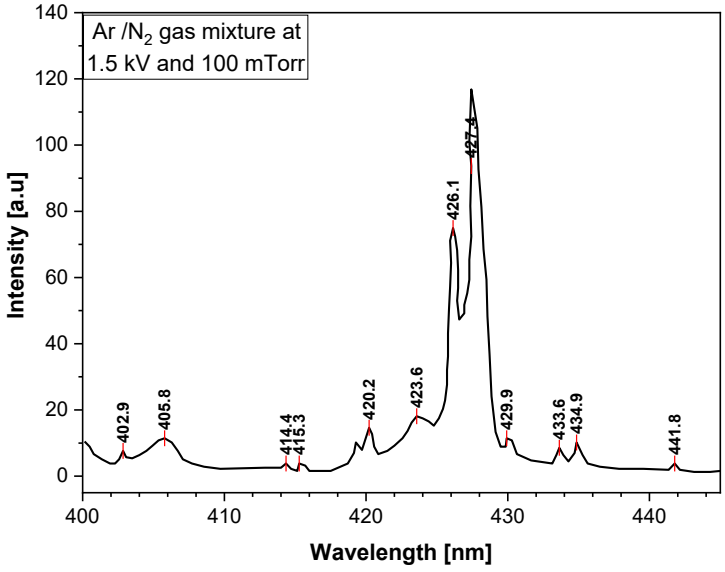

Figure 2. A scan of the optical emission spectrum of a DC hollow cathode discharge of Ar/N_2 gas mixture, recorded in the wavelength range of 400 nm to 445 nm, was obtained at a gas pressure of 100 mTorr and an applied voltage of 1.5kV.

Multidisciplinary Materials Chronicles, 2025, Vol. X, Iss. X, 140-149

DOI: 10.62184/mmc.jmmc1100202532

Research Article

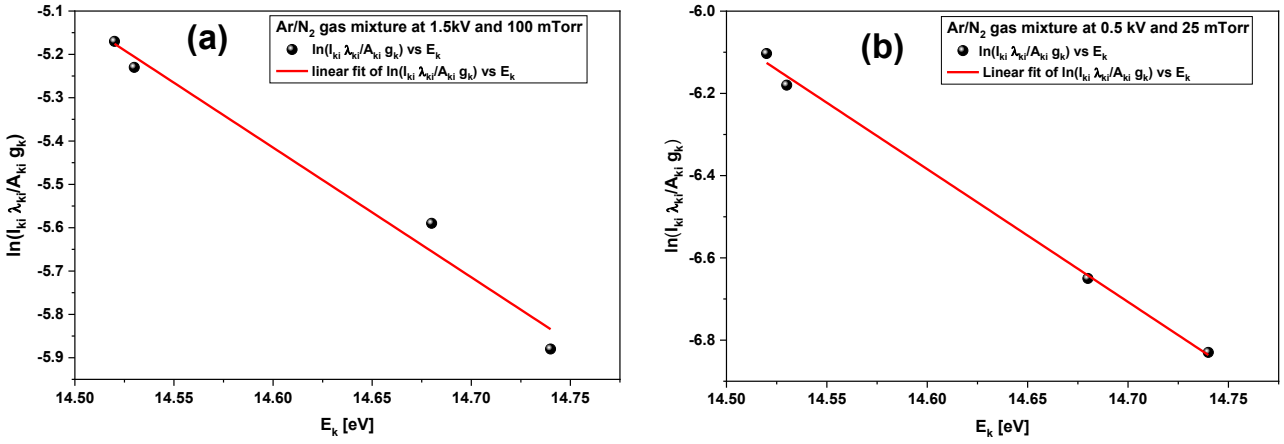

Figure 3. A Boltzmann plot for Ar/N_2 gas mixture DC hollow cathode discharge at (a) 1.5 kV applied voltage, and gas pressure 100 mTorr, and (b) 0.5 kV applied voltage, and gas pressure 25 mTorr.

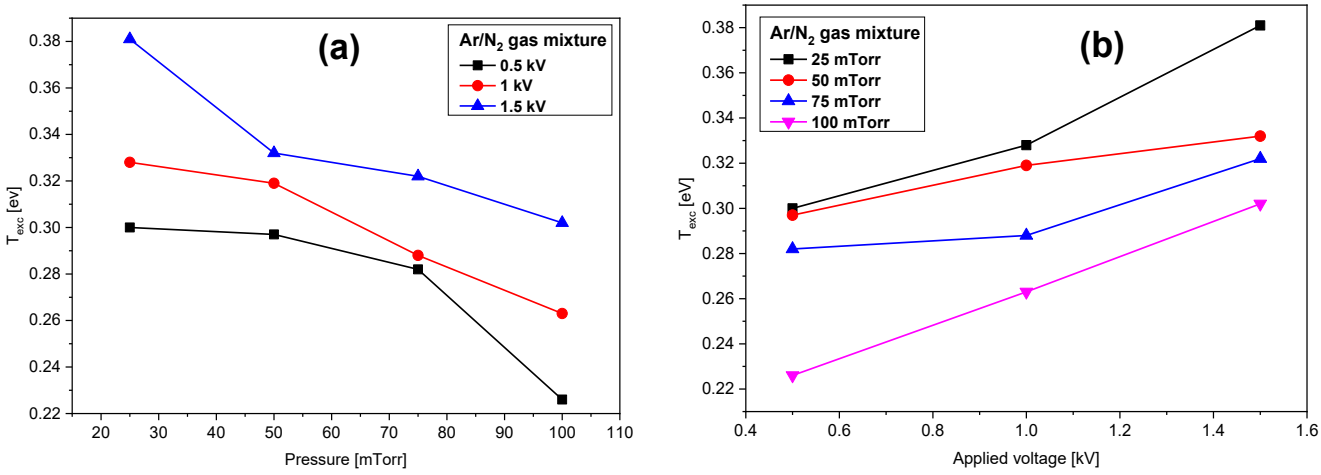

Figure 4. Excitation temperature T_{exc} of Ar/N_2 gas mixture plasma (a) as a function of gas pressures at different discharge voltages 0.5, 1, and 1.5 kV, and (b) as a function of applied discharge voltage at different gas pressures 25, 50, 75, and 100 mTorr.

Notable emission lines appear at 353.6 nm, 357.7 nm, 371.1 nm, 375.5 nm, 380.5 nm, 391.4 nm, 394.4 nm, 396.2 nm, and 399.8 nm. Among these, the 380.5 nm line corresponds to the SPS, while the 391.4 nm line is characteristic of the FNS. The FNS band at 391.4 nm is particularly intense and shows sharp band heads [30].

Figure 5b shows the spectrum for Ar/N_2 gas mixture at 1.5 kV and 100 mTorr, where the intensities of both SPS and FNS bands are enhanced. This increase is attributed to a higher population density of excited species, particularly those requiring two-step or two-electron excitation processes [31].

4.3. Effect of gas pressure on SPS and FNS Intensities

Figure 6 shows the variation of SPS and FNS intensities as a function of gas pressure at 1.5 kV (as an example). Contrary to expectations based on collisional excitation theory, which predicts reduced intensities due to energy loss from increased collisions, the observed intensities increase with pressure, where the SPS (380.5 nm) increased from 6.8 to 18, while the FNS (391.4 nm) increased from 58 to 82 as pressure increases from 25 mTorr to 100 mTorr.

Multidisciplinary Materials Chronicles, 2025, Vol. X, Iss. X, 140-149

DOI: 10.62184/mmc.jmmc1100202532

Research Article

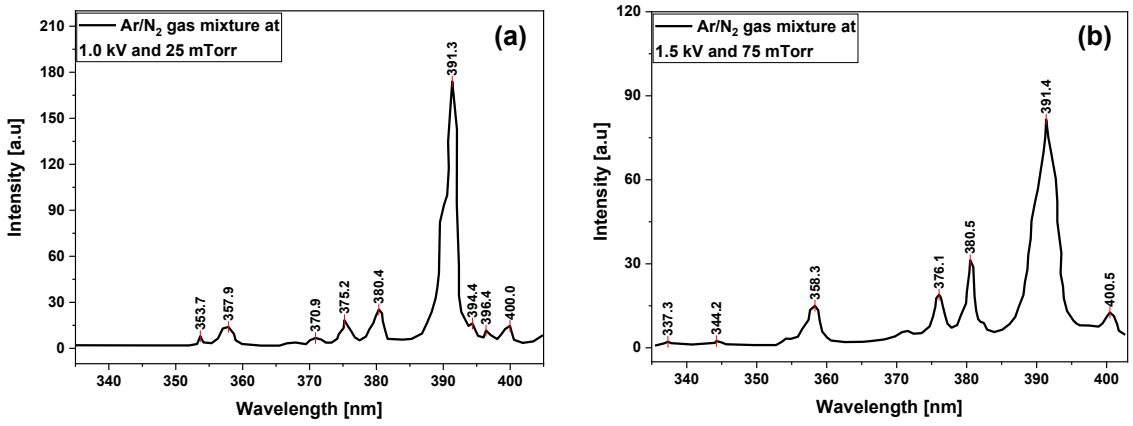

Figure 5. A scan of the optical emission spectrum of a DC hollow cathode discharge of an Ar/N_2 gas mixture was obtained at (a) applied voltage of 1 kV and pressure of 25 mTorr and (b) applied voltage of 1.5 kV and 75 mTorr.

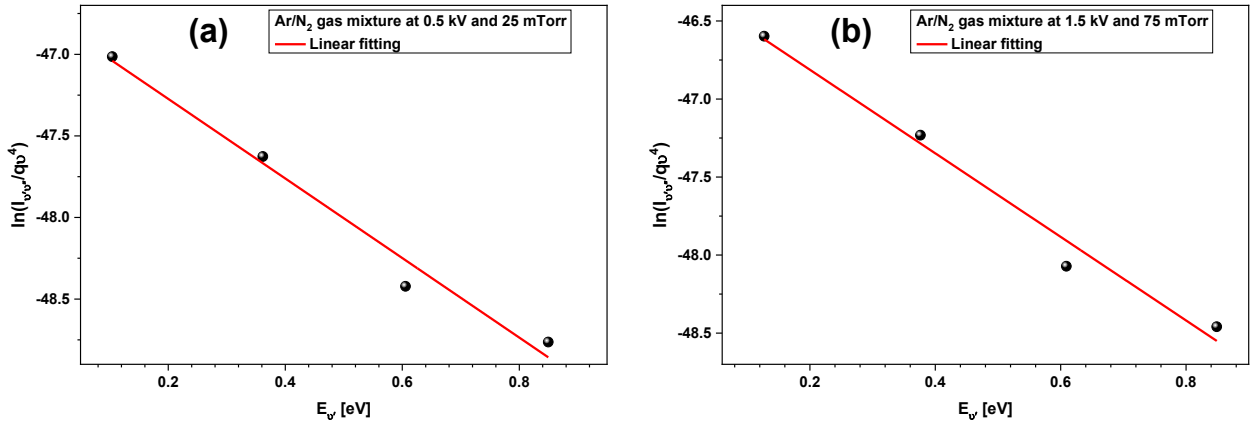

Figure 6. Boltzmann plot ($ln\ (I_{v'v"}/qv^4)$) vs vibrational energy for determining T_{vib} of Ar/ N_2 gas mixture at (a) 0.5 kV and 25 mTorr and (b) at 1.5 kV and 100 mTorr.

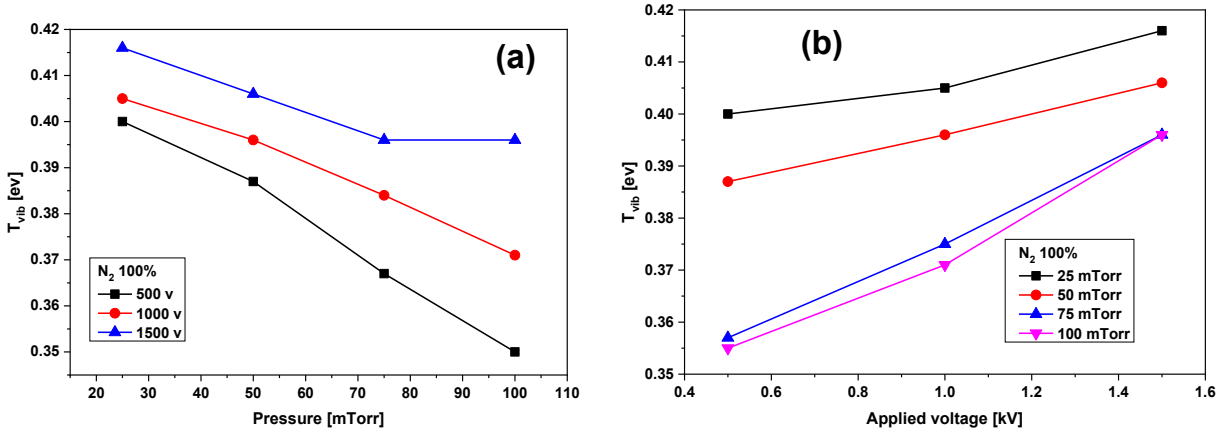

Figure 7. The plot of T_{vib} of N_2 as a function of (a) gas pressure at various applied voltages, 0.5, 1, and 1.5 kV, and (b) at various gas pressures, 25, 50, 75, and 100 mTorr.

DOI: 10.62184/mmc.jmmc1100202532

Research Article

This apparent contradiction is resolved by considering that two-step collisional processes and recombination mechanisms may become more significant at higher pressures, enhancing the population of excited states despite the increased collisional quenching [32].

4.4. Determination of vibrational temperature (T_{vib}) of N_2

The vibrational temperature of nitrogen was determined from SPS band intensities using the Boltzmann plot method (Equation 6), which involves plotting $\ln(I_{\upsilon'\upsilon''}/q\upsilon^4)$ versus the vibrational energy of the upper level. Figures 6a and 6b show representative Boltzmann plots under two conditions, 0.5 kV, 25 mTorr, and 1.5 kV, 100 mTorr (as an example). Four emission bands from the $\Delta\upsilon = -2$ sequence of the SPS ($C^3\Pi_u(\upsilon') \rightarrow B^3\Pi_g(\upsilon'')$) were selected (0,2) at 380.5 nm, (1,3) at 375.5 nm, (2,4) at 371.04 nm, and (3,5) at 367.08 nm.

This $\Delta\upsilon = -2$ sequence was chosen due to its long lifetime (~36 ns) [33], which minimizes radiative transfer effects and ensures more accurate temperature determination.

4.5. Dependence of vibrational temperature on gas pressure and voltage

Figure 7a presents the variation of T_{vib} as a function of gas pressure for various applied voltages. A decrease in T_{vib} from 0.416 eV to 0.35 eV is observed as the pressure increases from 25 mTorr to 100 mTorr. This trend is attributed to the increased frequency of collisions at higher pressure, which leads to energy loss and reduced vibrational excitation [34].

The dependence can also be interpreted through the relationship $E_k = eE\lambda_e$, where λ_e (the electron mean free path) is inversely proportional to pressure (P). Thus, increasing pressure shortens λ_e, resulting in lower energy transfer per collision and a corresponding drop in T_{vib} .

Figure 7b shows that increasing the applied voltage from 0.5 kV to 1.5 kV causes an increase in T_{vib} from 0.35 eV to 0.416 eV, due to enhanced electron energy and increased vibrational excitation efficiency [35].

4.6. Effect of argon addition on SPS and FNS intensities

Figure 8 illustrates the effect of argon concentration on the emission intensities of the SPS (380.5 nm) and FNS (391.4 nm) bands at 1.5 kV and 100 mTorr. As the Ar percentage increases from 10% to 50%, the intensity of the SPS increases (from 22 to 30), while that of the FNS decreases (from 137 to 75).

This behavior is explained by the increasing population of argon metastable states (Ar^*). The SPS radiative upper state (~11.1 eV) lies slightly below the energy levels of the metastable Ar states $3P_2$ (11.55 eV) and $3P_0$ (11.72 eV), facilitating Penning ionization and efficient population of the SPS levels [6].

In contrast, the FNS upper state (~18.7 eV) is energetically inaccessible for Penning ionization from Ar metastable, resulting in reduced population and emission.

4.7. Comparison of excitation and vibrational temperatures

A comparison between the T_{exc} and the T_{vib} reveals an interesting trend: under certain discharge conditions, T_{vib} values (ranging from 0.35 eV to 0.416 eV) appear to exceed T_{exc} values (ranging from 0.226 eV to 0.381 eV). This observation is counterintuitive, as excitation temperature, which characterizes electron impact excitation of atomic energy levels, is generally expected to be higher than molecular vibrational temperature due to the larger energy spacing of electronic transitions compared to vibrational ones. This discrepancy may stem from several factors: (i) potential overestimation of T_{vib} due to limited vibrational bands or deviations from the Boltzmann distribution under non-equilibrium conditions, (ii) underestimation of T_{exc} caused by line selection or uncertainties in spectroscopic constants, or (iii) inherent non-equilibrium characteristics of low-pressure plasmas, where high-energy electrons selectively excite vibrational levels while the overall average electron energy remains low [36].

5. Future work

Further investigation involving electron energy distribution function (EEDF) analysis, time-resolved spectroscopy, and expanded spectral diagnostics is recommended to clarify this behavior and ensure accurate thermodynamic interpretation.

DOI: 10.62184/mmc.jmmc1100202532

Research Article

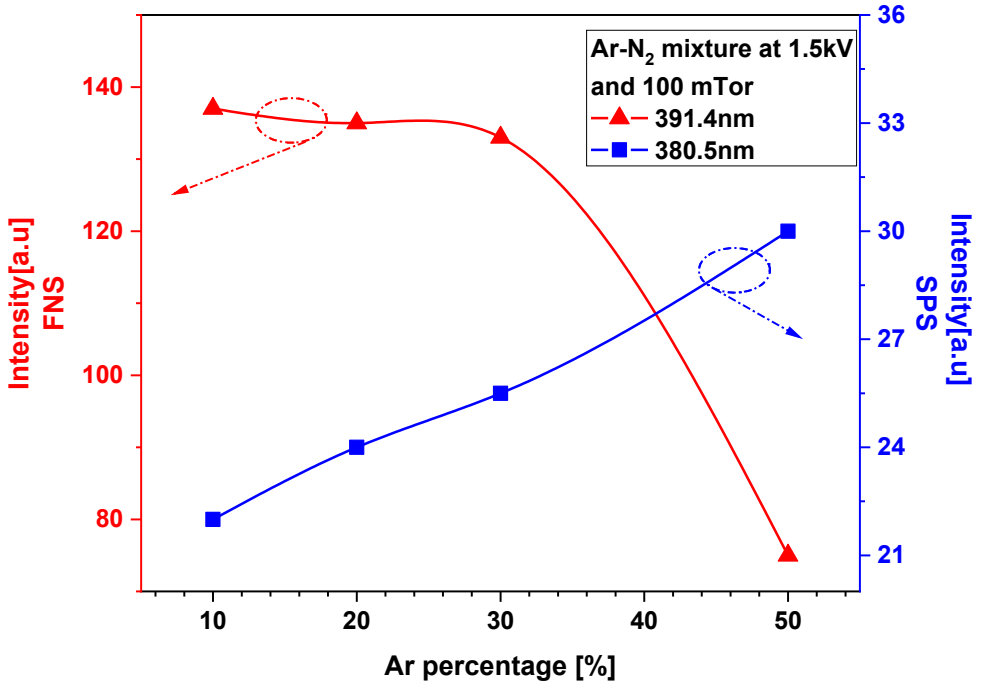

Figure 8. Spectral intensities of SPS and FNS of DC hollow cathode discharge for Ar/N_2 gas mixture as a function of Ar percentage at 1.5 kV and 100 mTorr.

6. Conclusion

This work presents a detailed spectroscopic characterization of Ar/N_2 plasmas in a DC hollow cathode discharge, focusing on the excitation and vibrational dynamics of argon and nitrogen species. The excitation temperature of Ar, derived via Boltzmann analysis, exhibited a strong dependence on both gas pressure and applied voltage, decreasing from 0.381 eV to 0.226 eV with rising pressure from 25 to 100 mTorr, and increasing from 0.226 eV to 0.381 eV as voltage rose from 0.5 kV to 1.5 kV. Optical emission features of the N_2 second positive system (SPS) and first negative system (FNS) were observed at 380.5 nm and 391.4 nm, respectively. The vibrational temperature (T_{vib}) of N_2, calculated from four $\Delta\upsilon = -2$ SPS bands, decreased from 0.416 eV to 0.35 eV with pressure increase and increased from 0.35 eV to 0.416 eV with higher voltage, aligning with theoretical predictions on electron energy and mean free path. The addition of argon to N_2 plasma enhanced SPS emission (from 22 to 30 intensity units) but suppressed FNS emission (from 137 to 75), attributable to selective Penning excitation due to Ar metastable (~11.55 eV). These results confirm the critical role of discharge parameters in modulating plasma properties for potential applications in thin film deposition and gas sensing.

Conflict of interest statement

The authors declare that they have no conflicts of interest.

Funding statement

This manuscript received no external funding.

Author information

Corresponding author: A.M. Hassan*

E-mail: a.m.hassan9214@gmail.com

Data availability

Data will be available on request.

References

[1] D.M. Goebel, G. Becatti, I.G. Mikellides, A.L. Ortega, Plasma hollow cathodes, J. Appl. Phys. 130 (2021) 050902. https://doi.org/10.1063/5.0051228.

[2] I.I. Beilis, The phenomenon of a cathode spot in an electrical arc: The current understanding of the mechanism of cathode heating and plasma generation, Plasma 7 (2024) 329–354. https://doi.org/10.3390/plasma7020019.

DOI: 10.62184/mmc.jmmc1100202532

[3] H. Baránková, L. Bardos, Hollow cathode and hybrid plasma processing, Vacuum 80 (2006) 688–692. https://doi.org/10.1016/j.vacuum.2005.11.047.

[4] M. Ahmed, M. Tisaev, S. Masillo, A. Lucca Fabris, Operational and plume properties of a modular hollow cathode for ground testing of plasma thrusters, J. Phys. D: Appl. Phys. 58 (2025) 285204. https://doi.org/10.1088/1361-6463/ade44f.

[5] N.C.M. Fuller, M.V. Malyshev, V.M. Donnelly, I.P. Herman, Characterization of transformer coupled oxygen plasmas by trace rare gases-optical emission spectroscopy and Langmuir probe analysis, Plasma Sources Sci. Technol. 9 (2000) 116–127. https://doi.org/10.1088/0963-0252/9/2/304.

[6] A. Qayyum, S. Zeb, M.A. Naveed, N.U. Rehman, S.A. Ghauri, M. Zakaullah, Optical emission spectroscopy of Ar–N_2 mixture plasma, J. Quant. Spectrosc. Radiat. Transf. 107 (2007) 361–371. https://doi.org/10.1016/j.jqsrt.2007.02.008.

[7] R.R. Arslanbekov, A. Kudryavtsev, R.C. Tobin, On the hollow-cathode effect: Conventional and modified geometry, Plasma Sources Sci. Technol. 7 (1998) 310–322. https://doi.org/10.1088/0963-0252/7/3/009.

[8] G. Stockhausen, M. Kock, Proof and analysis of the pendulum motion of beam electrons in a hollow-cathode discharge, J. Phys. D: Appl. Phys. 34 (2001) 1683. https://doi.org/10.1088/0022-3727/34/11/316.

[9] N. Martin, O. Banakh, A.M.E. Santo, S. Springer, R. Sanjinés, J. Takadoum, F. Lévy, Correlation between processing and properties of TiOxNy thin films sputter deposited by the reactive gas pulsing technique, Appl. Surf. Sci. 185 (2001) 123–133.

[10] M.M.A. El-Hadeed, M.E. Abdelkader, F.B. Diab, M.A. Al-Halim, Investigation of a coaxial pulsed plasma thruster by electrothermal discharge in Teflon propellant, CEAS Space J. (2025). https://doi.org/10.1007/s12567-025-00637-4.

[11] K.-B. Chai, D.-H. Kwon, Optical emission spectroscopy and collisional-radiative modeling for low temperature Ar plasmas, J. Quant. Spectrosc. Radiat. Transf. 227 (2019) 136–144. https://doi.org/10.1016/j.jqsrt.2019.02.015.

[12] P. Jamroz, W. Zyrnicki, Optical emission characteristics of glow discharge in the N_2–H_2–$Sn(CH_3)_4$ and N_2–Ar–$Sn(CH_3)_4$ mixtures, Surf. Coat. Technol. 201 (2006) 1444–1453. https://doi.org/10.1016/j.surfcoat.2006.02.013.

[13] M.M. Hefny, S.T. Abd El-latif, F.B. Diab, K.M. Ahmed, The contribution of electrode spacing and operating voltage on the time-resolved optical emission spectra of atmospheric-pressure air and Ar DBD plasma, Radiat. Eff. Defects Solids 179 (2024) 1569–1584. https://doi.org/10.1080/10420150.2024.2352842.

[14] J.L. Jauberteau, I. Jauberteau, Determination of the electron energy distribution function in weakly ionized plasma by means of a Langmuir probe and numerical methods, AIP Adv. 14 (2024) 055326. https://doi.org/10.1063/5.0204161.

[15] N. Bibinov, H. Halfmann, P. Awakowicz, Determination of the electron energy distribution function via optical emission spectroscopy and a Langmuir probe in an ICP, Plasma Sources Sci. Technol. 17 (2008) 035004. https://doi.org/10.1088/0963-0252/17/3/035004.

[16] F.U. Khan, N.U. Rehman, S. Naseer, M.Y. Naz, N.A.D. Khattak, M. Zakaullah, Effect of excitation and vibrational temperature on the dissociation of nitrogen molecules in Ar–N_2 mixture RF discharge, Spectrosc. Lett. 44 (2011) 194–202. https://doi.org/10.1080/00387010.2010.497527.

[17] P. Svarnas, Vibrational temperature of excited nitrogen molecules detected in a 13.56 MHz electrical discharge by sheath-side optical emission spectroscopy, Plasma Sci. Technol. 15 (2013) 891. https://doi.org/10.1088/1009-0630/15/9/11.

[18] P. Jamroz, W. Zyrnicki, Optical emission spectroscopy study for nitrogen–acetylene–argon and nitrogen–acetylene–helium 100 kHz and DC discharges, Vacuum 84 (2010) 940–946. https://doi.org/10.1016/j.vacuum.2009.12.019.

[19] P. Jamroz, W. Zyrnicki, A spectroscopic study into the decomposition process of titanium isopropoxide in the nitrogen–hydrogen 100 kHz low-pressure plasma, Vacuum 82 (2008) 651–656. https://doi.org/10.1016/j.vacuum.2007.10.003.

[20] H. Asghar, R. Ali, M.A. Baig, Determination of transition probabilities for the 3p → 3s transition array in neon using laser induced breakdown spectroscopy, Phys. Plasmas 20 (2013) 123302. https://doi.org/10.1063/1.4849436.

[21] X.L. Deng, A.Yu. Nikiforov, P. Vanraes, C. Leys, Direct current plasma jet at atmospheric pressure operating in nitrogen and air, J. Appl. Phys. 113 (2013) 023305. https://doi.org/10.1063/1.4774328.

[22] A.J. Wu, H. Zhang, X.D. Li, S.Y. Lu, C.M. Du, J.H. Yan, Determination of spectroscopic temperatures and electron density in rotating gliding arc discharge, IEEE Trans. Plasma Sci. 43 (2015) 836–845. https://doi.org/10.1109/TPS.2015.2394441.

[23] A.E. Metawa, F.M. El-Hossary, M. Raaif, M.H. Salaheldeen, A.A.A. El-Moula, Langmuir probe and optical emission spectroscopy studies for RF magnetron sputtering

DOI: 10.62184/mmc.jmmc1100202532

during TiON thin film deposition, Chin. J. Phys. 68 (2020) 168–177. https://doi.org/10.1016/j.cjph.2020.09.012.

[24] C. Ni, X. Cheng, Ab initio study of the second positive system of N_2 at high temperature, Comput. Theor. Chem. 1197 (2021) 113158. https://doi.org/10.1016/j.comptc.2021.113158.

[25] L. Ventura, C.E. Fellows, The N_2 second positive ($C^3\Pi \rightarrow B^3\Pi$) system reviewed: Improved data and analysis, J. Quant. Spectrosc. Radiat. Transf. 239 (2019) 106645. https://doi.org/10.1016/j.jqsrt.2019.106645.

[26] L. Ma, T. Yin, D. Li, P. Jiang, M. Cheng, H. Gao, Spectroscopic study of a new electronic band system $^{33}\Delta g–a^3\Pi u$ of C_2, J. Phys. Chem. A 128 (2024) 1074–1084. https://doi.org/10.1021/acs.jpca.3c07734.

[27] N.U. Rehman, F.U. Khan, M.A. Naveed, M. Zakaullah, Determination of excitation temperature and vibrational temperature of the $N_2(C^3\Pi u, \nu')$ state in Ne–N_2 RF discharges, Plasma Sources Sci. Technol. 17 (2008) 025005. https://doi.org/10.1088/0963-0252/17/2/025005.

[28] K.M. Ahmed, F.B. Diab, W.H. Gaber, F.A. Ebrahim, M.E. Abdel-Kader, Experimental investigation of a low-energy linear plasma propulsion device, Jpn. J. Appl. Phys. 59 (2020) 106001. https://doi.org/10.35848/1347-4065/abb2e3.

[29] M.M. Vojnović, M.M. Ristić, Resonant effects of electron transport in MW E(t) × DC B fields: Vibrational excitation of N_2, Plasma Sources Sci. Technol. 34 (2025) 055014. https://doi.org/10.1088/1361-6595/adda77.

[30] J.J. Camacho, J.M.L. Poyato, L. Díaz, M. Santos, Optical emission studies of nitrogen plasma generated by IR CO_2 laser pulses, J. Phys. B: At. Mol. Opt. Phys. 40 (2007) 4573. https://doi.org/10.1088/0953-4075/40/24/003.

[31] M. Rudolph, A. Revel, D. Lundin, N. Brenning, M.A. Raadu, A. Anders, T.M. Minea, J.T. Gudmundsson, On the population density of the argon excited levels in a high power impulse magnetron sputtering discharge, Phys. Plasmas 29 (2022) 023506. https://doi.org/10.1063/5.0071887.

[32] R.C. Bolden, R.S. Hemsworth, M.J. Shaw, N.D. Twiddy, The measurement of Penning ionization cross sections for helium 2^3S metastables using a steady-state flowing afterglow method, J. Phys. B: At. Mol. Phys. 3 (1970) 61. https://doi.org/10.1088/0022-3700/3/1/014.

[33] X.-M. Zhu, Y.-K. Pu, Determining the electron temperature in inductively coupled nitrogen plasmas by optical emission spectroscopy with molecular kinetic effects, Phys. Plasmas 12 (2005) 103501. https://doi.org/10.1063/1.2061587.

[34] H.L. Davies, V. Guerra, M. van der Woude, T. Gans, D. O'Connell, A.R. Gibson, Vibrational kinetics in repetitively pulsed atmospheric pressure nitrogen discharges: Average-power-dependent switching behaviour, Plasma Sources Sci. Technol. 32 (2023) 014003. https://doi.org/10.1088/1361-6595/aca9f4.

[35] F. Grätz, D.P. Engelhart, R.J. Wagner, H. Haak, G. Meijer, A.M. Wodtke, T. Schäfer, Vibrational enhancement of electron emission in CO ($a^3\Pi$) quenching at a clean metal surface, Phys. Chem. Chem. Phys. 15 (2013) 14951–14955. https://doi.org/10.1039/C3CP52468J.

[36] M. Aflori, D.G. Dimitriu, D. Dorohoi, Characterization of argon–oxygen discharge using Langmuir probe and optical emission spectroscopy measurements, Plasma Phys. 28 (2004) 2–5.